

## **Dome C site characterization in 2006 with Single Star Scidar**

Christophe Giordano, Jean Vernin, Merieme Chadid, Eric Aristidi and Abdelkrim Agabi  
Université de Nice-Sophia Antipolis, Observatoire de la Côte d'Azur, CNRS-UMR7293, Lab.  
Lagrange, 06108 Nice Cedex 2, France

Hervé Trinquet

DGA Matrise de l'information, BP 7 35998 RENNES ARMEES, France

cgordano@oca.eu, vernin@unice.fr, chadid@unice.fr, aristidi@unice.fr,  
agabi@unice.fr, herve.trinquet@dga.defense.gouv.fr

Received \_\_\_\_\_; accepted \_\_\_\_\_

## ABSTRACT

We present observations made in 2006 with the Single Star Scidar (SSS) at Dome C in Antarctica, allowing us to determine optical turbulence  $C_N^2(h)$  as well as velocity  $\mathbf{V}(h)$  profiles from ice level up to **about 25 km above sea level (a.s.l.)**. SSS is a 16-inch telescope placed on an equatorial mount tracking continuously Canopus star. About **90000** individual profiles are analyzed from March to September, where surface layer contribution to seeing can be separated from the rest of the atmosphere. Medians of high angular resolution parameters relevant to astronomy are statistically studied, such as seeing (1.0 arcsec), isoplanatic angle (6.9 arcsec) and wavefront coherence time (3.4 ms). For a telescope placed above the turbulent surface layer superb conditions are encountered (**medians of seeing better than 0.3 arcsec, isoplanatic angle better than 6.9 arcsec and coherence time larger than 10 ms**). Astronomical conditions are twice better at the beginning of the night with  $\varepsilon_0 \approx 0.5arcsec$ ,  $\theta_0 \approx 11.5arcsec$  and  $\tau_0 \approx 15ms$ . SSS wind velocity profiles are consistent with National Oceanic and Atmospheric Administration analysis **up to 17km (a.s.l.), within a  $\pm 2ms^{-1}$  error bar**. **Coherence étendue**, which is a combination of  $\varepsilon_0$ ,  $\theta_0$  and  $\tau_0$ , well adapted to adaptive optics performances, is likely **4 times** better at Dome C than at the already known observatories **such as Mauna Kea or ORM**.

*Subject headings:* Astronomical Phenomena and Seeing

## 1. Introduction

Dome C is a plateau in Antarctica, at latitude  $75^{\circ}$  south. It lies 1000 km inland at an altitude of 3233 m. Since its opening in 2005, the Italy-French Concordia station is of great interest for research, especially for astronomy. Indeed the main advantage of Antarctica is the almost continuous night during the polar winter ( $\sim 3$  months), allowing continuous observation of the same field of view. Moreover the atmospheric turbulence at Dome C seems to be very advantageous because this site is unique having a very strong but very thin turbulent surface layer,  $\sim 30$  m thick, much less than the  $\sim 200$  m surface layer lying above “classical” observatories and even at South Pole (Agabi et al. 2006, Marks et al. 1999). **These characteristics have also been verified using a numerical simulation of atmospheric turbulence (Lascaux et al. 2011)**

Since 2005, the astronomical community seeks to characterize the sky above Dome C (Lawrence et al. 2004, Agabi et al. 2006, Vernin et al. 2007, Trinquet et al. 2008, Aristidi et al. 2009), with instruments such as DIMM, MASS, SODAR, sounding balloons and more recently with Single Star Scidar (SSS) (Vernin et al. 2009) **or with numerical model (Lascaux et al. 2011)**. We will focus here on data collected by SSS during the 2006 winter campaign. SSS technique is used at Dome C because the classical Scidar (double star) requires a telescope with a pupil larger than 1 m, which is not available at Dome C (Hoegemann et al. 2004 and references therein).

Vernin et al. 2009 presented the first results obtained at Dome C with the SSS, restricted to two nights. They validate the instrument by comparison with a DIMM and National Oceanic and Atmospheric Administration<sup>1</sup> archive, showing good agreement for seeings ranging from 0.2 to 2 arcsec and for wind velocities. In next part 2, we briefly recall the Scidar principle and improvements in detectivity threshold calculation. In section 3, the results on the statistical

---

<sup>1</sup><http://ready.arl.noaa.gov/READYamet.php>

distribution, the stability and seasonal evolution of integrated parameters such as seeing  $\varepsilon_0$ , coherence time  $\tau_0$ , isoplanatic angle  $\theta_0$  and "coherence étendue"  $G_0$  are discussed as well as  $C_N^2(h)$  and  $\mathbf{V}(h)$  profiles. In section 4 the small approximation assumption is discussed and Dome C is compared with other "classical" mid-latitude observatories and South Pole.

## 2. Single Star Scidar method

### 2.1. Brief recall

**SSS is based on a 40cm telescope Ritchey-Chrétien optical combination supported by an equatorial mount (see more details in Vernin et al. 2009). The whole instrument is designed to resist to the worst polar conditions.**

SSS technique calculates spatio-temporal correlation of images of the scintillation of single star  $C_*(\mathbf{r}, t)$ . The autocorrelation has a single bump at the center. Cross-correlations may have several bumps displaced from the center of the correlation plane with different amplitudes. Each bump corresponds to a turbulent layer (Vernin & Azouit 1983):

- The width of each bump depends upon the altitude and the wind velocity dispersion  $\sigma_v$  of the corresponding layer;
- The bump position depends upon the wind speed and wind direction  $\mathbf{V}$ ;
- The amplitude of the bump depends upon the intensity of turbulence  $C_N^2$ ,  $h$  and  $\sigma_v$ .

**The vertical resolution of SSS is  $dh = 500m$ . It can reach a maximum altitude of about 30 km along the line of sight, but considering that the airmass of Canopus star varies between 1.2 and 1.6, the maximum altitude reached by SSS is about 25 km a.s.l. in our case.**

**The first detectable wind speed is  $\Delta V = \sec z \cdot \Delta x / 2\Delta T \approx 1.5ms^{-1}$  (Vernin et al. 2009),**

and the maximum detectable wind speed is comprised between 35 and  $49\text{ms}^{-1}$ , as detailed in section 2.2.2.

## 2.2. Data filtering

### 2.2.1. Coherence surface depending upon wind speed

In order to calculate the vertical profiles of  $C_N^2(h)$ ,  $\mathbf{V}(h)$ , and  $\sigma_v(h)$ , we use a simulated annealing algorithm which is described by Habib et al. 2006. This algorithm generates a large number of atmospheric configuration sets  $\{C_N^2, V_x, V_y, \sigma_v\}_{h_i}$ , at each altitude  $h_i$ , in order to find one that gives an autocorrelation and a cross correlation as close as possible to the real correlations  $C_*(\mathbf{r}, 0)$ ,  $C_*(\mathbf{r}, \Delta t)$  and  $C_*(\mathbf{r}, 2\Delta t)$  (Vernin et al. 2009), where  $\Delta t$  is the time lag between two adjacent images of the pupil. **SSS adds 4 sub-layers at zero altitude because we found several bumps in the correlation plan corresponding to very low altitude layers (less than the SSS resolution). If one wants to take into account these bumps, corresponding to surface layer, it is necessary to add about 4 sub-layers at zero altitude.** Examples of results obtained with this method are shown in Figs 1 and 2 which represent the temporal evolution of the profile of  $C_N^2(h)$  and  $\mathbf{V}(h)$ . One can see spurious velocity evaluations in Fig. 2 (top), which seems very noisy and with many very high velocities. **These spurious velocities coincide most of the time with very low optical turbulence level.**

In order to clean out the velocity pattern, we now focus on the detectivity threshold of SSS. As was shown by Vernin & Azouit 1983, and Vernin et al. 2009, the  $C_N^2$  detectivity threshold of SSS is given by:

$$\Delta(C_N^2 \delta h) = 0.042 C_*(O) \frac{\lambda^{17/12} h^{-7/12}}{\sqrt{DN}} \quad (1)$$

where  $\delta h$  is the thickness of the turbulent layer, D is the diameter of the telescope, N the number

of images, and  $C_*(0)$  the variance of scintillation:

$$C_*(0) = \sigma_I^2 = 19.2\lambda^{-7/6} \int_0^\infty h^{5/6} C_N^2 dh. \quad (2)$$

This formula is true if we assume that the image is infinite, which is not the case in practice. When the scintillation pattern displacement due to wind speed becomes large when compared to the pupil size, the surface of coherence of the pupil decreases, which implies that the statistical error increases. To calculate the detectivity threshold, we use the real number of speckles observed in this surface of coherence (Vernin & Azouit 1983):

$$\frac{\Delta C_*}{C_*(0)} = \frac{1}{\sqrt{n_{speckles}}} = \sqrt{\frac{\rho}{DN}} \quad (3)$$

where  $\rho$  is the first Fresnel zone, it is the diameter of the spatial correlation of the scintillation  $\rho = 0.67 \sqrt{\lambda h}$ .

Equation 3 is true when one calculates the auto-correlation where all the atmospheric speckles participate to the evaluation of  $C_*(\mathbf{r})$  as well as the spatio-temporal cross-correlation  $C_*(\mathbf{r}, \tau)$  for zero velocity turbulent layers. Let us imagine now a turbulent layer crossing the pupil within a time  $\approx 2\Delta t$ . When evaluating the cross-correlation at  $\tau = 2\Delta t$ , almost no speckle will contribute to the evaluation of  $C_*(\mathbf{r}, 2\Delta t)$ , leading to a poor signal to noise ratio. In last equation 3, one needs to take into account the effective number  $n$  of speckles which participate to the cross-correlation computation:

$$n_{speckles} = N_{speckles} \frac{S}{S_0} \quad (4)$$

where  $N_{speckles}$  is the number of speckles observed within the whole collecting light surface  $S_0$  (the surface of the pupil), corresponding to a zero velocity, and  $S$  is the coherence surface for the calculation of cross correlation corresponding to a non zero velocity ( $S$  **depends upon velocity of**

**each layer**). The detectivity threshold to consider **for each altitude** is now:

$$\Delta(C_N^2 dh) = 0.042 C_*(O) \frac{\lambda^{17/12} h^{-7/12}}{\sqrt{DN}} \sqrt{\frac{S_0}{S}}. \quad (5)$$

### 2.2.2. *Speckles going outside the pupil*

Since the diameter  $D$  of pupil is limited to  $40\text{cm}$ , the measurable wind speed is also limited. The maximum distance between a bump and the center of the correlation plane can not exceed  $D$ . This speed limit depends on the diameter of the pupil, and the time interval  $2\Delta t$  between three images:

$$V_{max} = \frac{D}{2\Delta t}. \quad (6)$$

**For SSS at Dome C,  $2\Delta t = 11.2\text{ms}$ , then  $V_{max} \approx 35\text{m/s}$  perpendicularly to the line of sight. If we consider  $secz \approx 1.4$  with Canopus star at Dome C, the velocity measured in  $y$  direction must be corrected in order to obtain the horizontal wind speed. Therefore  $V_{y_{max}}$  can reach  $49\text{ms}^{-1}$ . In other words, depending on the wind velocity direction, the maximum detectable wind modulus is comprised between  $35$  and  $49\text{ms}^{-1}$ .**

Why two intervals? Habib et al. 2006 have shown that the simulated annealing method needs the knowledge of the auto and the first two cross-correlations measured at  $\Delta t$  and  $2\Delta t$ , in order to separate the bump widening effect due to both the altitude  $h$  and the velocity dispersion  $\sigma_V$ . Therefore, one needs to filter all the data that have wind velocities greater than  $V_{max}$ .

The detectivity threshold of SSS detailed in section 2 affects mainly the high speeds, and therefore essentially the coherence time  $\tau_0$  which is the only integrated parameter depending upon wind speed (equation 9). In Fig. 3, we compared the evaluation of the wavefront coherence time

$\tau_0$  before and after the filtering process. One can see that the coherence time is slightly greater when this filtering is applied because spurious high wind velocities have been rejected.

Once the two filtering are performed, one can assess atmospheric parameters important for adaptive optics.

### 3. Results

In order to characterize the atmosphere from an observational point of view, it is necessary to calculate the seeing  $\varepsilon_0$ , the isoplanatic angle  $\theta_0$ , and the coherence time  $\tau_0$ . These parameters can be calculated using the vertical profiles of  $C_N^2$ , and wind speed  $\mathbf{V}$  (Roddiier 1981):

$$\varepsilon_0 = 5.25\lambda^{-1/5} \left[ \int_{h_0=8m}^{\infty} C_N^2(h)dh \right]^{3/5} \quad (7)$$

$$\theta_0 = 0.058\lambda^{6/5} \left[ \int_{h_0=8m}^{\infty} h^{5/3} C_N^2(h)dh \right]^{-3/5} \quad (8)$$

$$\tau_0 = 0.058\lambda^{6/5} \left[ \int_{h_0=8m}^{\infty} |\mathbf{V}(h)|^{5/3} C_N^2(h)dh \right]^{-3/5} \quad (9)$$

where  $h$  is the altitude above the telescope and  $h_0$  is the SSS elevation above ice,  $h_0 = 8m$ .

From these parameters, one can calculate the "coherence étendue"  $G_0 = r_0^2\tau_0\theta_0^2$  as defined by Lloyd 2004, where Fried's parameter  $r_0$  (Roddiier 1981) is directly deduced from the seeing:

$$r_0 = \frac{0.98\lambda}{\varepsilon_0}. \quad (10)$$

This parameter is important because it is a weighting of the three main integrated parameters  $\varepsilon_0$ ,  $\theta_0$  and  $\tau_0$ , well adapted to adaptive optics.

**For SSS, the surface layer corresponds to the 4 sub-layers at the zero-altitude, and the free atmosphere correspond at any other layer (from 1 km above ice level).**

All the results shown here were calculated from about 90000 profiles measured between March and September 2006. In order to decrease the computation time (simulated annealing method requires huge computation), we averaged each set of 10 profiles, leading to about 9000 profiles, the repartition of which is shown in fig 7.

### 3.1. Statistical distributions

After calculating these parameters, we studied their statistics to see how they are distributed. The statistical distribution of the high angular resolution parameters is shown in Fig. 4 with normalized histograms.

On the top left, we can see the distribution of seeing  $\varepsilon_0$ . This graph shows that the seeing varies between 0.1 and 3.5 arcsec, with a slightly bi-modal distribution: the first bump appears around 0.4 arcsec and the second at 1.2 arcsec. The dashed line corresponds to the cumulative distribution showing that half of the time the seeing is better than 1 arcsec. The bi-modal trend of the seeing have been also observed by Aristidi et al. 2009 at Dome C.

The isoplanatic angle (top right ) follows a log-normal distribution with an average and a median values of respectively 7.78 and 6.91 arcsec. The coherence time (bottom left) follows a log-normal distribution with an average and a median values of respectively 4.90 and 3.43 ms. The coherence étendue (bottom right) follows a log-normal distribution with an average and a median values of respectively 40.6 and  $1.8 \text{ m}^2.\text{ms}.\text{arcsec}^2$ .

### 3.2. Parameters stability

The stability of these parameters is of major concern and can be estimated from continuous time during which one can make an acquisition with a parameter better than a given value. As an

example, what is the normalized continuous time  $\mathcal{T}$  during which  $\varepsilon_0 < \varepsilon'_0$ ? Since observations are made over time intervals which may vary from few minutes to hours, we took into account the duration of these intervals to compute some normalized fraction of time comprised between 0 and 1:

$$\mathcal{T}(\varepsilon'_0) = \frac{\sum_{i=1}^{i=M} t_{i,j}(\varepsilon'_0)}{\sum_{j=1}^{j=N} t_j} \quad (11)$$

where  $j$  refers to one of the  $N$  continuous observations,  $t_{i,j}(\varepsilon'_0)$  is the duration of one of the  $M$  intervals of time where the constraint  $\varepsilon_0 < \varepsilon'_0$  is true during the  $j^{\text{th}}$  record and  $t_j$  is the duration of the  $j^{\text{th}}$  record. With that definition, the stabilities of  $\varepsilon_0$ ,  $\theta_0$ ,  $\tau_0$  and  $G_0$  are shown in Fig. 5.

Considering the whole atmosphere contribution, at  $\mathcal{T} = 0.5$ , the seeing is continuously better than 1.2 arcsec, the isoplanatic angle is continuously larger than 6 arcsec, the coherence time is continuously larger than 3 ms and the coherence étendue is continuously larger than 1.2  $m^2.ms.arcsec^2$ . Considering only the free atmosphere contribution, the threshold parameters (at  $\mathcal{T} = 0.5$ ) are respectively 0.3 arsec, 6 arcsec (same as previous case), 8.5 ms and 40  $m^2.ms.arcsec^2$ .

Another way to estimate the stability is to compute the evolution of the four integrated parameters during the 18 hours of the polar night, centered on the local midnight and averaged (and median) over the whole 2006 campaign, as shown in Fig. 6. One can notice large differences between median and mean  $\tau_0$  and  $G_0$  values due to the large scattering of these variables.

One can see that astronomical conditions are much better at the beginning of observation, from 6 to 9 UT, and then deteriorate and remain stabilized during the rest of the night, from 9 to 24 UT, 16 UT corresponding to local midnight.

### 3.3. Seasonal Evolution of parameters

In order to know the evolution of the atmospheric quality during the year, we also calculated the average, month by month, of each integrated parameter. The result is visible in the Fig. 7. The continuous line represents the average over the whole atmosphere and the dashed line refers to the free atmosphere.

The evolution of  $\theta_0$  is calculated only for the whole atmosphere because this parameter is insensitive to the lower layers.

### 3.4. Vertical profiles and wind speed evolution

Fig. 8 shows the **average** profiles of  $C_N^2(h)$ ,  $|\mathbf{V}(h)|$  **over whole atmosphere and within the surface layer**. The top-left graph shows the **average** profile of optical turbulence  $C_N^2$ . **The bottom-left graph shows  $C_N^2$  values within the surface layer. It is clear that almost all the turbulence is concentrated in the lower altitude layers. The top right** graph is the vertical profile of wind speed modulus  $|\mathbf{V}(h)|$  calculated with SSS (solid line). The dashed line represents the horizontal velocity modulus calculated with NOAA archive. **The bottom-right graph shows values of horizontal wind velocity modulus within the surface layer sorted with increasing velocities.** One can see that the modulus of wind speed calculated by SSS and NOAA are rather close within the low stratosphere, but they differ at higher altitudes when  $h_{asl} > 17$  km.

In order to know the evolution of wind speed during the year, we computed the monthly average of the mean horizontal velocity, averaged over the whole atmosphere, deduced from SSS and NOAA data. The result is shown in Fig. 9. The trend of the two curves is similar, but NOAA velocities are slightly larger than SSS ones. The mean wind speed of the slowest surface layer detected by the SSS is around 6 m/s, at 8 m above ice level, also observed by Travouillon et al. 2008. **Based on Meso-NH simulations, Lascaux et al. 2011 and Hagelin et al. 2008 found a**

wind speed above ice level of about 4 and  $8\text{ms}^{-1}$  respectively, which are very close to our SSS measurements.

#### 4. Discussion

In most of studies relevant to wave propagation, it is implied that the weak perturbation assumption is valid within the following constraint (Roddier 1981):

$$\sigma_I^2 = 19.12\lambda^{-7/6} \int_0^\infty h^{5/6} C_N^2(h) dh \leq 0.7 \quad (12)$$

where  $I$  is the normalized intensity fluctuation. SSS measures the autocorrelation of the scintillation  $C_*(\mathbf{r})$  in the pupil plane and gives access to the scintillation index  $\sigma_I^2 = C_*(0)$ . In Fig. 10, one can notice that equation 12 is well verified, with  $\sigma_I^2$  median being 0.14 and  $\sigma_I^2 \leq 0.4$  during the whole campaign. The distribution of the scintillation index seems to follow a log-normal curve, with a small secondary bump for  $\sigma_I^2 = 0.06$  which should correspond to the bi-modal shape of the seeing distribution shown in Fig. 4. No linear relationship can be given between the seeing and the scintillation index since the seeing is related to  $\int C_N^2(h) dh$  and the scintillation index to  $\int h^{5/6} C_N^2(h) dh$ .

Table 1 compares<sup>2</sup> the high angular resolution parameters found at Dome C with the same ones encountered in various other observatories. **We also calculated these parameters only during the winter (May to August), as suggested by the referee, but results are quite identical to the March-September period, and therefore values appearing in Table 1 refer to the whole**

---

<sup>2</sup>Aklim, ORM, Ventarrones and Macon are four sites which have been analysed in the framework of the European Extremely Large Telescope site survey published by Vernin et al. 2011. Armazones and Mauna Kea (M-K) site evaluation can be found in Schöck et al. 2009 and South Pole (S-P) in Marks et al. (1999)

**SSS observing period.** The seeing and the coherence time are poorer at Dome C, meanwhile the isoplanatic angle and the resulting coherence étendue are better. This feature can be explained by the particular atmospheric conditions at Dome C. Almost all the optical turbulence is concentrated within the surface layer where the strong potential temperature gradient is mixed by strong vertical wind shear, inducing a lot of seeing. Wind speed increases steeply from 5 to 10  $ms^{-1}$  from 8 to 30 m elevation, inducing low coherence time (see equation 9) when compared to “classical” observatories where the wind speed is lower in the surface layer. Isoplanatic angle is much larger at Dome C because almost all the optical turbulence is concentrated at  $h \approx 0$  with no influence on  $\theta_0$ , as seen in equation 8.

Finally, the coherence étendue, being sensitive to  $\theta_0^2$ , outperforms classical observatories.

We tried to apply the model detailed by Racine 2005 (equation 1) to Dome C conditions, and found that the predicted seeings for an elevation of 8 m and 30 m are respectively 0.66 and 0.65 arcsec, which are far from the 1.00 and 0.29 arcsec seeings of our study. But this author noticed that, at the time of his publication, Dome C conditions “critically depends on the still unmeasured SL contribution”.

After calculation of the average and median values of different atmospheric parameters (Fig. 4), one can notice that the distributions of  $\theta_0$ ,  $\tau_0$ , and  $G_0$  have a log-normal shape. One knows that a positive random variable might follow a quasi-Gaussian shape if its fluctuations remain small when compared to its mean. But, with larger fluctuations, the distribution becomes log-normal and even exponential in case of very large fluctuations. For example, the mean and median values of  $G_0$  are respectively 1.8 and  $40.6m^2.ms.arcsec^2$ , i.e a one to twenty two ratio, due to multiplicative effects of  $\varepsilon_0$ ,  $\theta_0$  and  $\tau_0$  fluctuations.

Looking at the graphs of stability of Fig. 5, one can see the huge improvement in adaptive optics condition if one excludes the surface layer contribution.

For what concern wind speed, in the bottom-left panel of Fig. 8, it seems that SSS and NOAA agree well up to the low stratosphere, from **the ice level** up to about 15 km. **Indeed SSS is an instrument which measures the optical turbulence, so if there is wind, but no optical turbulence, it can not measure the wind velocity. This case is possible when the gradient of potential temperature is stronger than the gradient of wind speed, because the Richardson number become large if  $\frac{1}{T} \frac{d\theta}{dh} \gg \frac{1}{g} (\frac{dV_h}{dh})^2$  as one can see from equation 13. This phenomenon is common at Dome C (see Geissler & Masciadri 2006) . This is one possible explanation to the weak velocities detected by SSS at high altitude whereas values obtained by Geissler & Masciadri 2006 are stronger.**

$$R_i = \frac{g}{T} \frac{\frac{d\theta}{dh}}{(\frac{dV_h}{dh})^2}. \quad (13)$$

**In order to verify that this underestimation has an influence or not on values of coherence time, we used the wind speed from the NOAA above 17km up to 25km a.s.l.(see fig. 8) to recalculate the coherence time. The median and average value obtained using NOAA wind modulus are respectively 3.4 and 4.8ms. These values are approximately the same that those obtained when one uses only the SSS measurements (3.4 and 4.9ms). Now, if we consider only the free atmosphere, the median and mean value of coherence time are respectively 9.8 and 16.1ms which is close of SSS values (10.2 and 18.5ms). Since high altitude  $C_N^2$  are very low at Dome C, the underestimation of the wind velocity has almost no influence on coherence time.**

Lets one imagine that it is possible to install a telescope at Dome C above the surface layer, i.e about 30 m above ice level, and see what are the consequences on main high angular resolution parameters. This idea was already suggested by Lawrence et al. 2004 because they measured these parameters with instruments (MASS and SODAR) which are not sensitive to the first 30 m of atmosphere. Later, Trinquet et al. 2008 shown the great importance of the surface layer

Param. \ Site	Site							
	Aklim	ORM*	Venta.	Macon	Armaz.	M-K	S-P	D-C
Total seeing $\varepsilon_0$ (arcsec)	1.00	0.80	0.80	0.87	0.64	0.75	1.6	1.00
FA seeing $\varepsilon_{FA}$ (arcsec)	0.52	0.31	0.55	0.66	0.43	0.33	0.32	0.29
SL seeing $\varepsilon_{BL}$ (arcsec)	0.77	0.65	0.60	0.51	0.35	0.54	1.53	0.90
Isoplan. angle $\theta_0$ (arcsec)	1.29	1.93	1.96	1.37	2.04	2.69	3.23	6.9
Coherence time $\tau_0$ (ms)	3.53	5.58	4.90	3.37	4.60	5.1	1.58	3.4
FA coher. time $\tau_{FA}$ (ms)	-	-	-	-	-	-	-	10.2
BL coher. time $\tau_{BL}$ (ms)	-	-	-	-	-	-	-	4.0
Coher. étendue $G_0$	0.05	0.38	0.26	0.10	0.49	0.62	0.07**	1.8
FA coher. étendue $G_0$	-	-	-	-	-	-	-	64
BL coher. étendue $G_0$	-	-	-	-	-	-	-	2.5

Table 1: Global median values of seeing, isoplanatic angle, time coherence of the wavefront, optical étendue, free atmosphere seeing and surface layer seeing.  $G_0$  is expressed in  $m^2ms^2arcsec^2$  unit.

\*ORM is Observatorio Roque de los Muchachos. 0.07\*\* is deduced from median values of  $\varepsilon_0$ ,  $\theta_0$  and  $\tau_0$  at South Pole (S-P). M-K is for Mauna Kea and D-C for Dome C.

contribution to optical turbulence at Dome C, confirming the steady free atmosphere above the thin surface layer. In Fig. 11, histograms and cumulative distribution of  $\varepsilon_0$ ,  $\theta_0$ ,  $\tau_0$  and  $G_0$  are given excluding the surface layer contribution. One can see that the seeing becomes excellent around 0.3 arcsec, the isoplanatic angle is the same since the surface layer contribution has no influence, the coherence time is about three times better with a median  $\tau_0$  about 10 ms and finally the coherence étendue is far better because  $G_0$  median is about  $64 \text{ m}^2 \text{ ms arsec}^2$ . Comparison of our measurements with those of Lawrence et al. 2004 and Trinquet et al. 2008 is given in Table 2. Our seeings compare well with Lawrence et al. 2004 estimation, but SSS isoplanatic angle and coherence time are larger by a factor **1.5-2.5**.

## 5. Conclusion

The purpose of this study is to characterize the quality of the atmosphere above Dome C from the point of view of high angular resolution astronomy. Single star scidar allows us to retrieve both  $C_N^2(h)$  and  $\mathbf{V}(h)$  profiles from ice level up to high atmosphere, giving access to the major high angular resolution parameters relevant to adaptive optics such as  $\varepsilon_0$ ,  $\theta_0$  and  $\tau_0$  and consequently to the coherence étendue  $G_0$ . Measurements were performed during the whole polar winter 2006, from March to September. The present analysis is based on a previous article from Vernin et al. (2009) where SSS and DIMM were cross-compared at the same time and same site, giving almost identical seeing measurements within a large dynamical range from 0.2 to 2.0 arcsec seeings. SSS-deduced wind speed measurements also well compared with National Oceanic and Atmospheric Administration re-analysis.

We have shown that the seeing follows a slightly bimodal distribution centered around 0.4 and 1.2 arcsec, mainly attributed to a major contribution of the surface layer optical turbulence. But, from time to time, its contribution disappears, leading to the only influence of the free atmosphere which is very steady and low. Over a seven months period, (March to September) the median

values of seeing, isoplanatic angle, coherence time and coherence étendue are respectively 1.00 arcsec, 6.9 arcsec, 3.43 ms and  $1.8 \text{ m}^2 \text{ ms arcsec}^2$ . These astronomical conditions well compare with other major astronomical sites such as ORM, Ventarrones<sup>3</sup>, Armazones<sup>4</sup> or Mauna Kea<sup>5</sup>.

Now that it is well established that most of the turbulence at Dome lies within the first 30 m above ice, it is tempting to imagine that a telescope might be placed onto a 30 m elevated platform, preventing from the turbulent surface layer. PILOT is such an attempt detailed by Lawrence et al. 2009 where the telescope is installed on top of a concrete-metallic pillar. Great care has to be taken to do not disturb the flow around the structure. Trinquet et al. 2008 shown that the gradient of the potential temperature at Dome C is about  $30^\circ\text{C}$  within 30 m, meaning a very strong vertical gradient of the refractive index. Any mechanical turbulence will produce strong optical turbulence, not only in the wake of the building structure but also above the building. Assuming that no extra turbulence is generated and installing the telescope above the surface layer, one would expect a median seeing, an isoplanatic angle and a coherence time of respectively 0.29 arcsec, 6.9 arcsec and 10.2 ms leading to a coherence étendue of  $64 \text{ m}^2 \text{ ms arcsec}^2$ , around ten time better than all the major known observatories.

We also demonstrated that the continuous time during which some integrated parameter is better than a given threshold, is much better above the surface layer than at ice level, except for the isoplanatic angle which is not affected by surface turbulence.

Surprisingly, the first hours of each 24 hour local night allows much better astronomical

---

<sup>3</sup>Ventarrones was selected as a potential site to install the European Extremely Large Telescope (E-ELT).

<sup>4</sup>Armazones was characterized in the framework of the Thirty Meter Telescope (TMT) project (Schöck et al. (2009) and 11 subsequent articles in PASP), but selected to install the E-ELT.

<sup>5</sup>Mauna Kea was finally selected to shelter the TMT.

conditions than in the middle and the end of the night. Indeed, one would expect equal condition regardless the hour of the night since the sun is always under the horizon. But the elevation angle of the sun varies from  $-8^\circ$  to  $-38^\circ$  below horizon allowing perhaps some disturbance on the gradient of the refractive index. During polar summer, Aristidi et al. 2005 have shown such phenomenon: the afternoon seeing remains below 0.5 arcsec for 5 continuous hours and then deteriorates. During the night and the morning, when the sun is low upon the horizon, the gradient of the potential temperature is very high and positive, and any kinetic energy induced by the flow creates very strong refractive index fluctuations. During the afternoon, the sun heats the surface layer air until the gradient of the potential temperature becomes zero. At this time, even in presence of kinetic energy, parcels of air of the same refractive index are mixed leading to  $C_N^2 \approx 0$ , and the only contribution to seeing comes from the free atmosphere.

Here, we confirm the rapid acceleration of the wind speed within the surface layer from 5 m/s at ground level up to about 10 m/s on top. Across the free atmosphere, **the wind speed measured by SSS is close to that measured by the NOAA up to 17km a.s.l. Above, SSS seems to underestimate the wind speed, but, at Dome C, this fact has almost no influence on other parameters.**

We wish to thank the technical staff of Fizeau laboratory for its help in all aspects of SSS setting up. The members of the Antarctica Dome C station are warmly thanked as well as the Paul Emile Victor institute which helped us in strategic decision and infrastructure. The French “Institut National des Sciences de l’Univers” granted the construction of the Dome C SSS prototype. National Oceanic and Atmospheric Administration is acknowledged for access to its meteorological re-analysis profiles through its ARL archive. Other technical aspects of the SSS have been made possible in the framework of the contract #F61775-02-C0002 with the US Air Force EOARD.

–SSS– DOMEK 20/03/2006 12:40:08 aca20m–10.rntt 2.5\*seuil

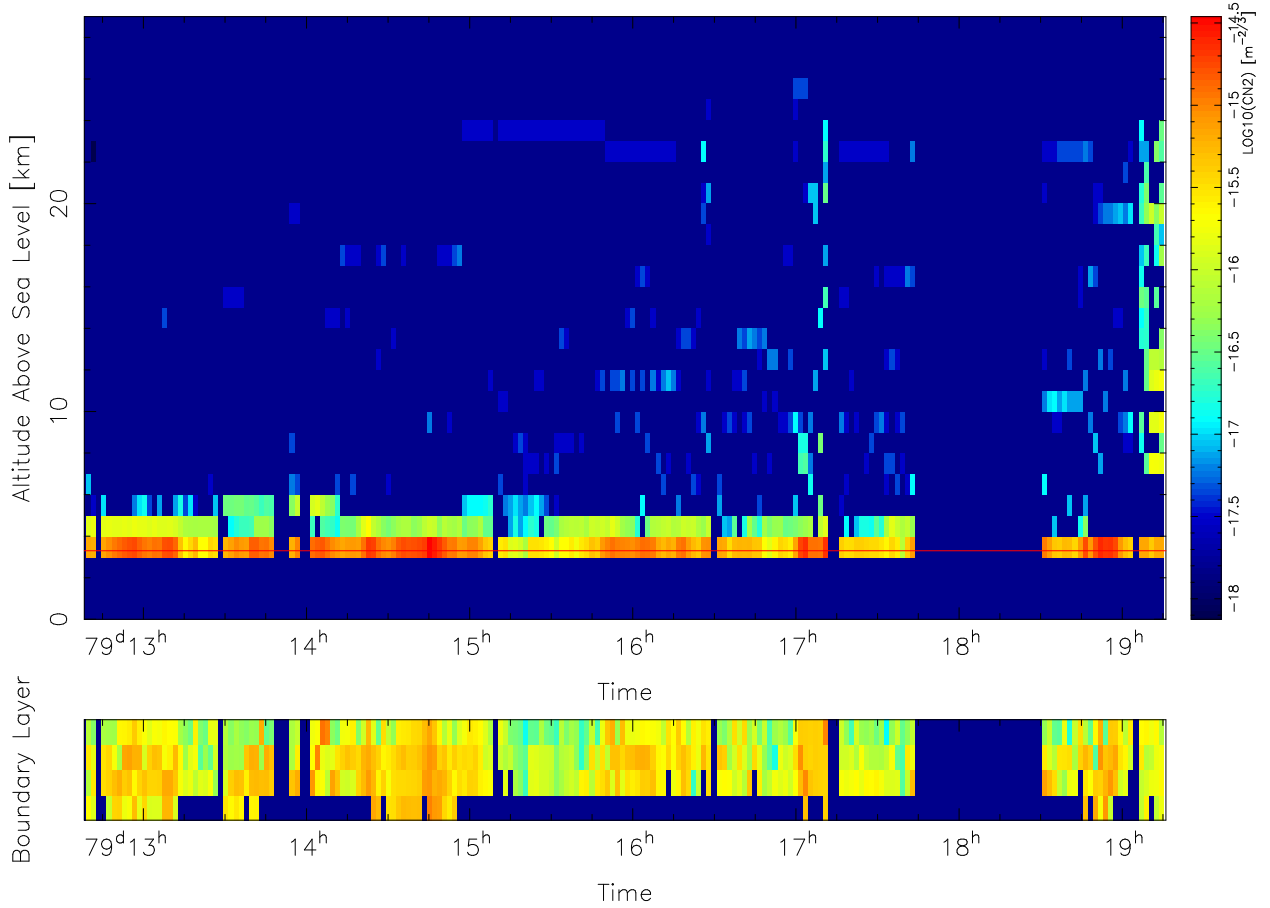
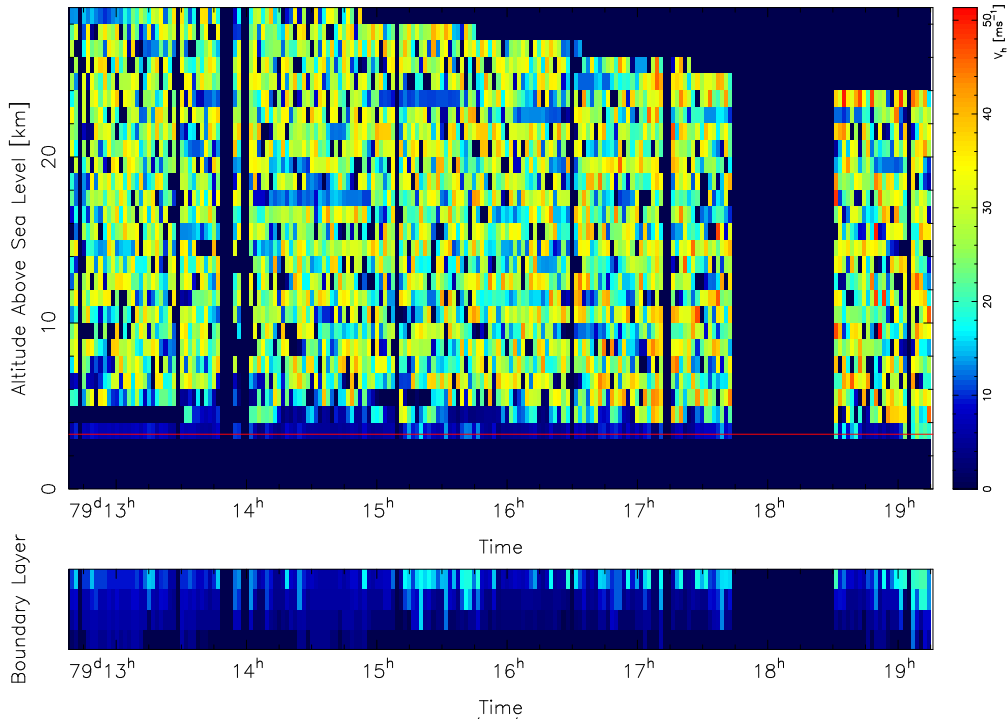


Fig. 1.— Example of vertical profile of  $C_N^2$  as a function of time obtained with SSS for March 20, 2006. The lower frame shows the  $C_N^2$  profile of the four sub-altitudes of the surface layer (see more explanations in Vernin et al. 2009). We notice that, above the surface layer there is almost no turbulence.

–SSS– DOMEK 20/03/2006 – Without filtering



–SSS– DOMEK 20/03/2006 – With filtering

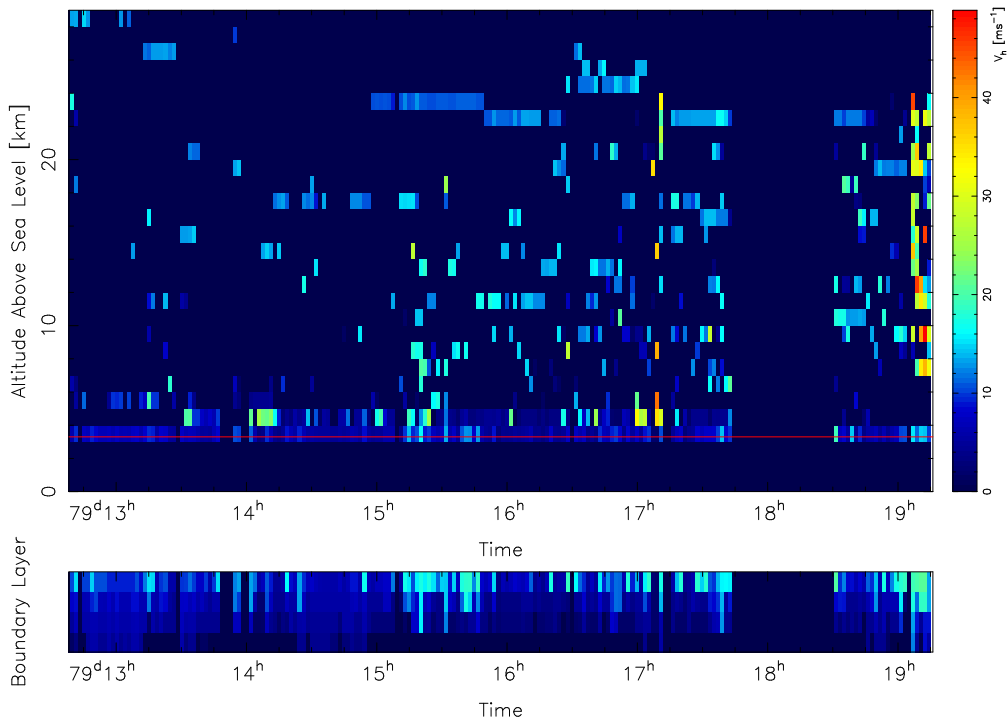


Fig. 2.— Example of vertical profile of horizontal velocity versus time obtained with SSS for March 20, 2006. Top: before filtering, bottom: after filtering (see text). In each figure, the lower frame shows the  $|\mathbf{V}(h)|$  profile of the four sub-altitudes of the surface layer (see more explanations in Vernin et al. 2009).

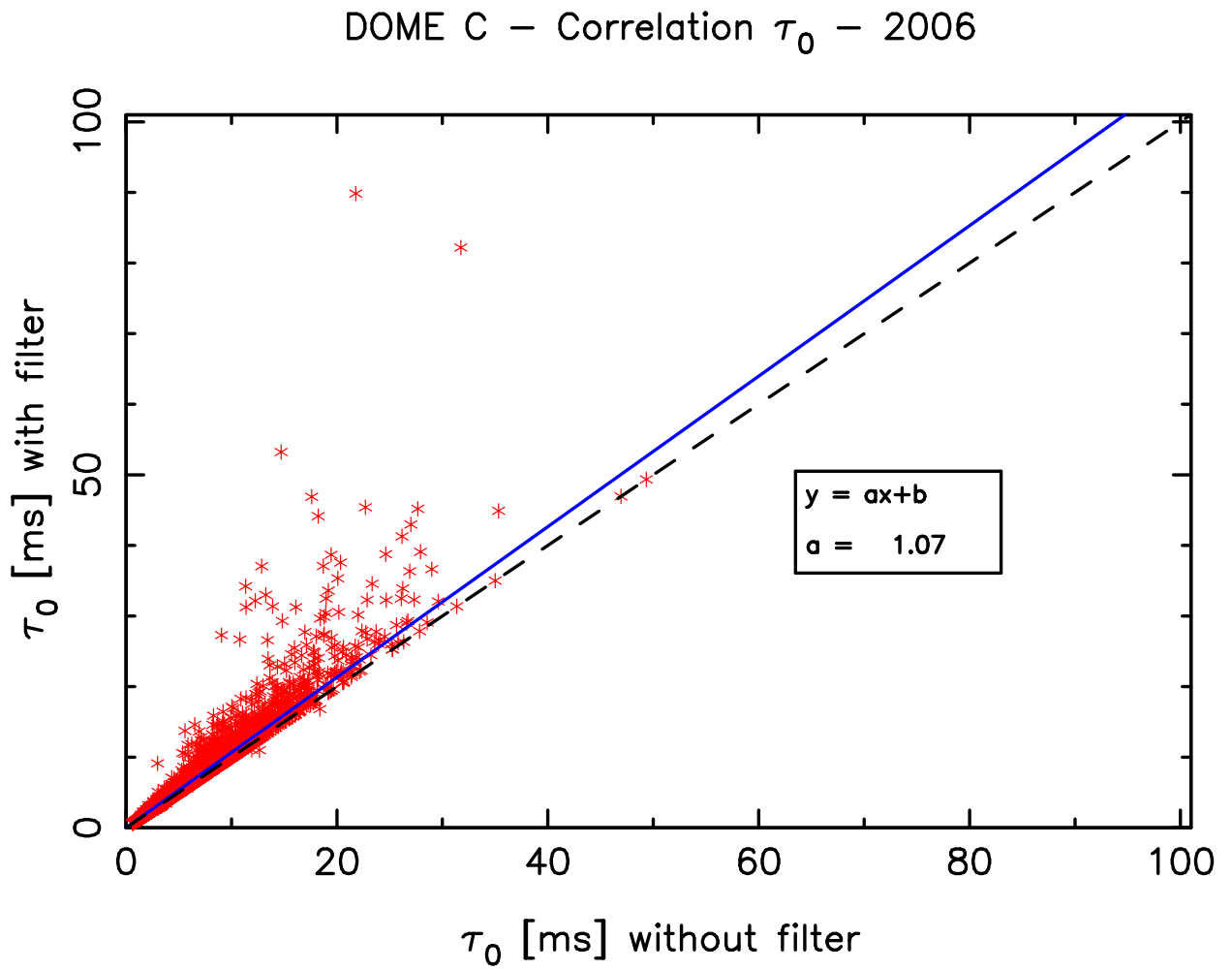


Fig. 3.— Correlation between the values of  $\tau_0$  obtained with and without filtering the data, depending on the wind speed (see explanation in the text).

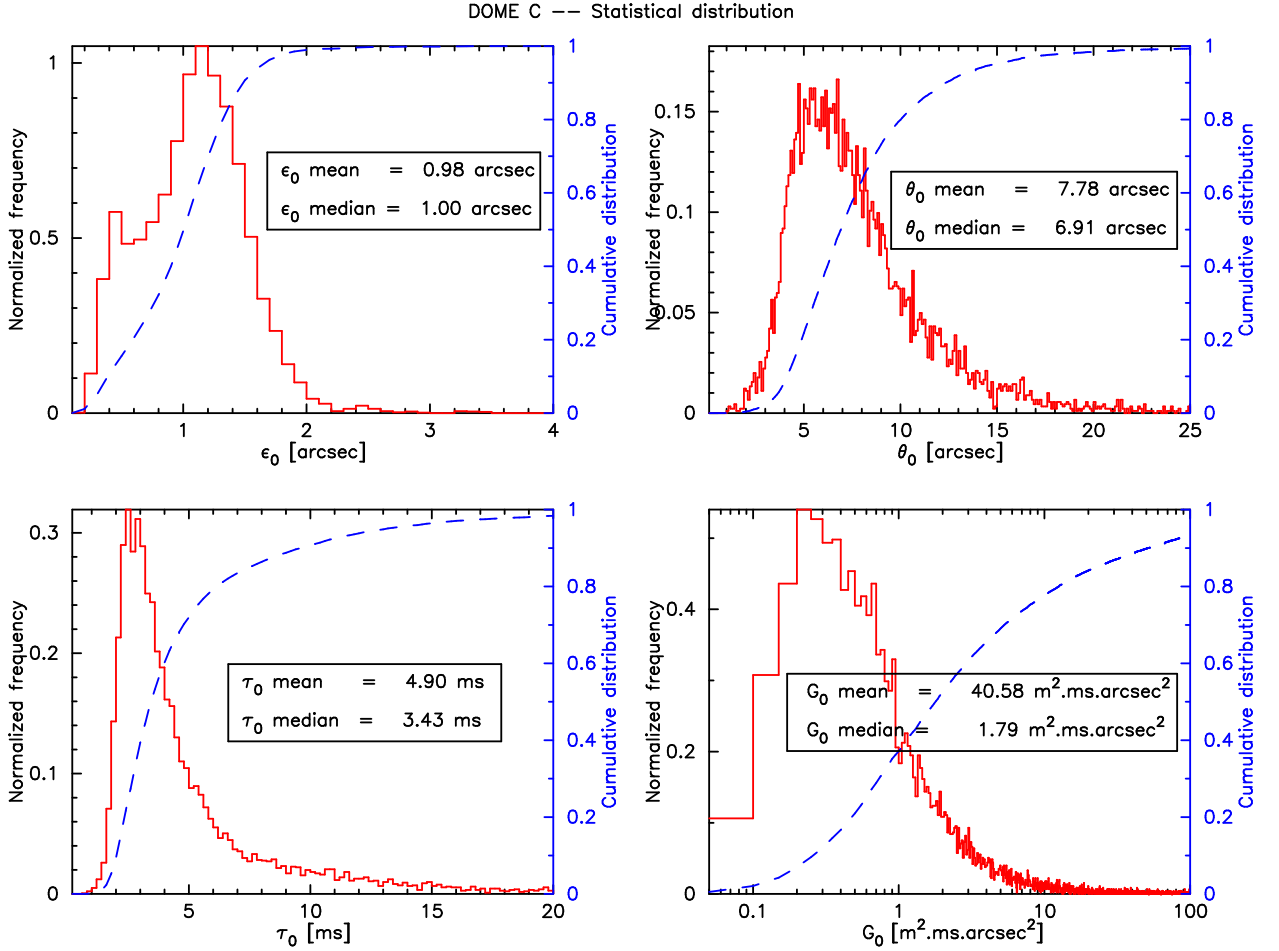


Fig. 4.— Histogram (line) and cumulative (dashed line) distribution of atmospheric parameters computed with SSS, from March to September 2006. Top left: distribution of seeing  $\epsilon_0$ . One can see a slightly bi-modal distribution. The other frames give the distributions of  $\theta_0$  (top right),  $\tau_0$  (bottom left), and  $G_0$  (bottom right). As expected from positive parameters, their distribution looks like log-normal.

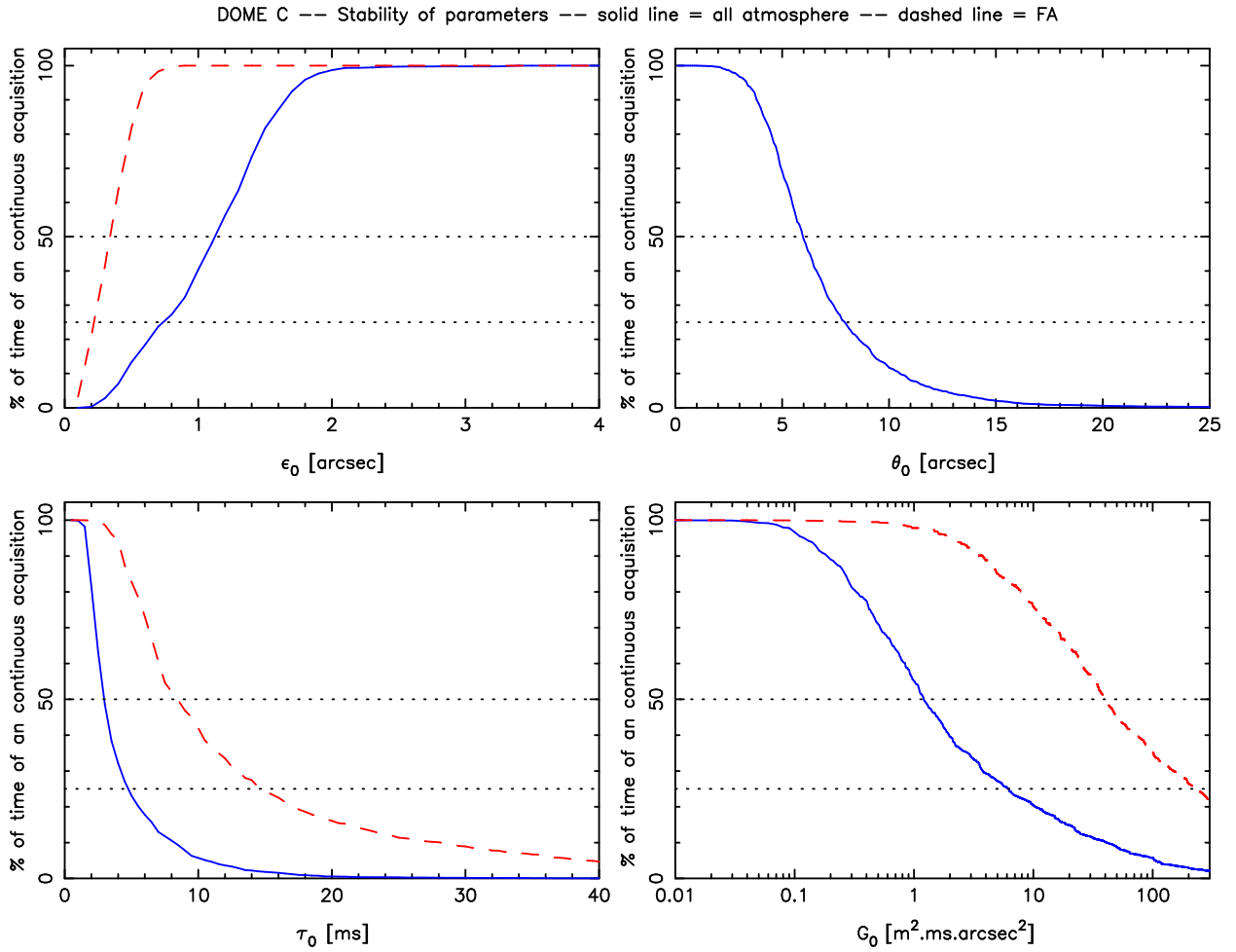


Fig. 5.— Stability of atmospheric parameters given by the percentage of continuous time  $\mathcal{T}$  during which an integrated parameter  $x$  follows the constraint ( $x < x'$ ) (see eq:11). From left to right and top to bottom: stability of  $\epsilon$ , stability of  $\theta_0$ , stability of  $\tau_0$  and stability of  $G_0$ . Continuous line refers to the whole atmosphere, dashed to the free atmosphere only.

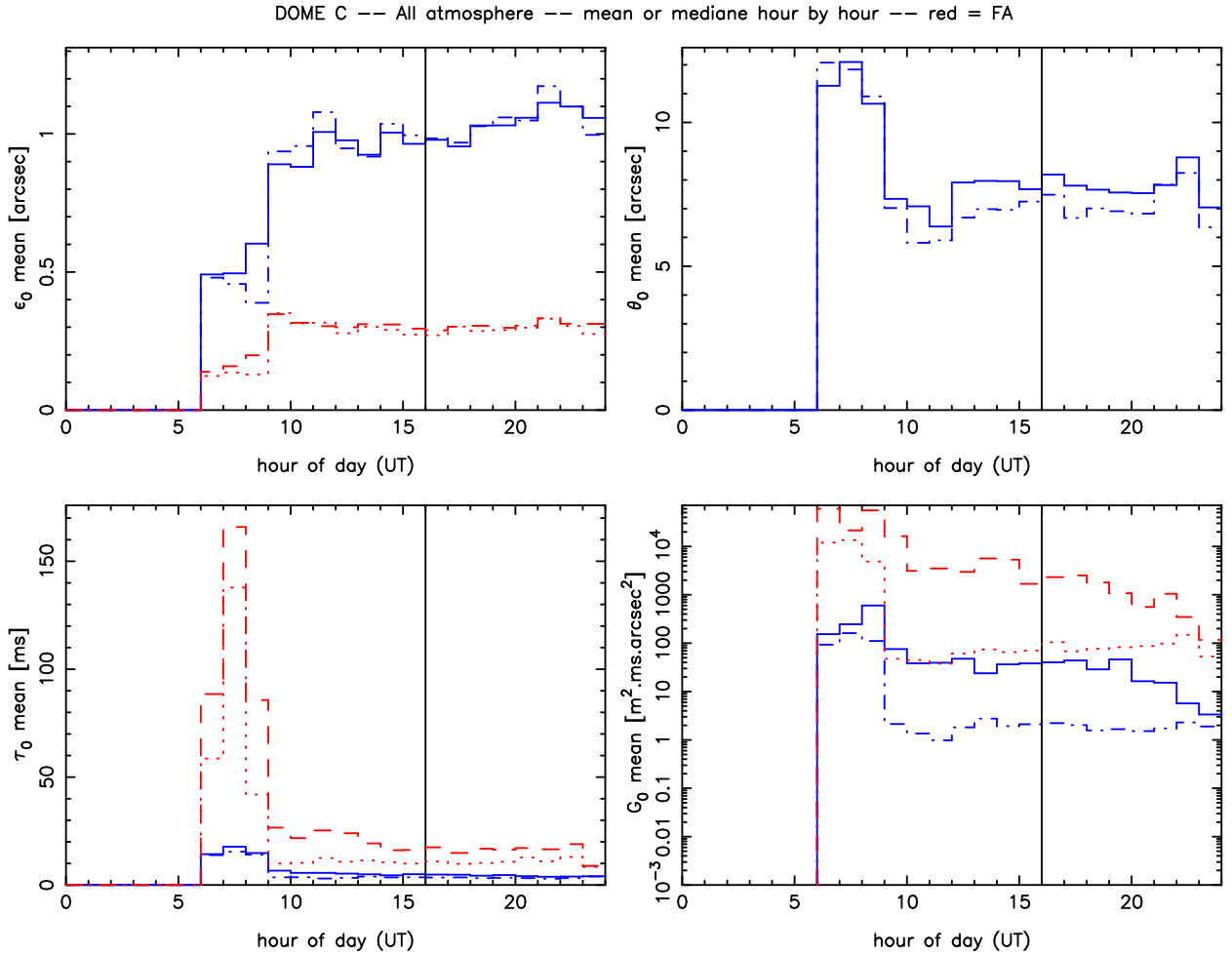


Fig. 6.— Mean (solid line) or median (dashed line) hour per hour of atmospheric parameters ( $\epsilon_0$  (top left),  $\theta_0$  (top right),  $\tau_0$  (bottom left),  $G_0$  (bottom right)) calculated over the whole atmosphere, for 2006 campaign. Mean (dots) and median (dot-dash) refers to the same parameters, but calculated over the free atmosphere. The early part of the night is more favorable for astronomical observation. The vertical line represents midnight in UT time.

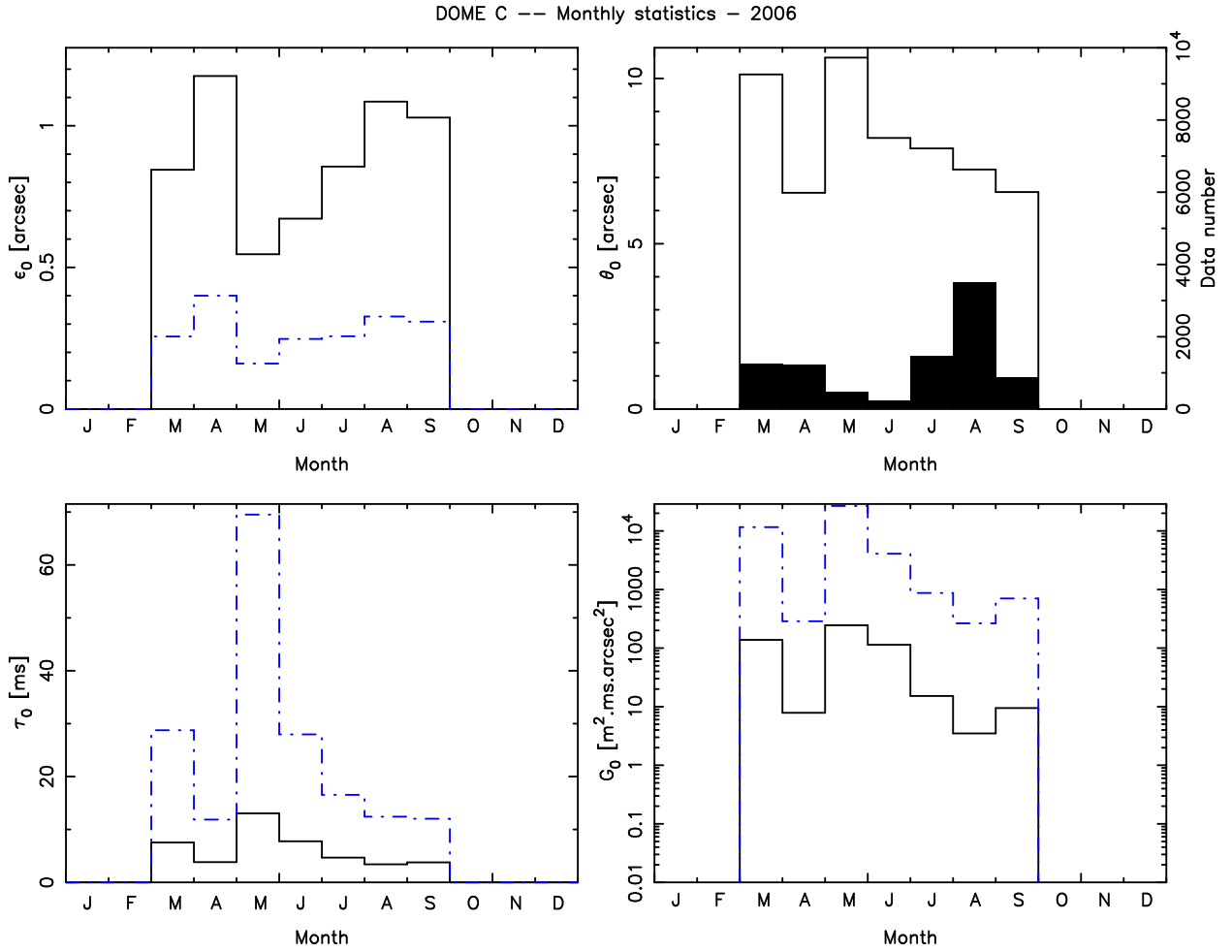


Fig. 7.— Seasonal evolution of **the median** of atmospheric parameters  $\epsilon_0$  (top left),  $\theta_0$  (top right),  $\tau_0$  (bottom left), and  $G_0$  (bottom right). Continuous curve is the evolution of parameters calculated over the whole atmosphere. Dashed line is the evolution of parameters calculated over the free atmosphere.  $\theta_0$  is insensitive to the lower layers (equation 8) and therefore it's insensitive to the surface layer. **The top right full histogram shows the distribution of profiles.**

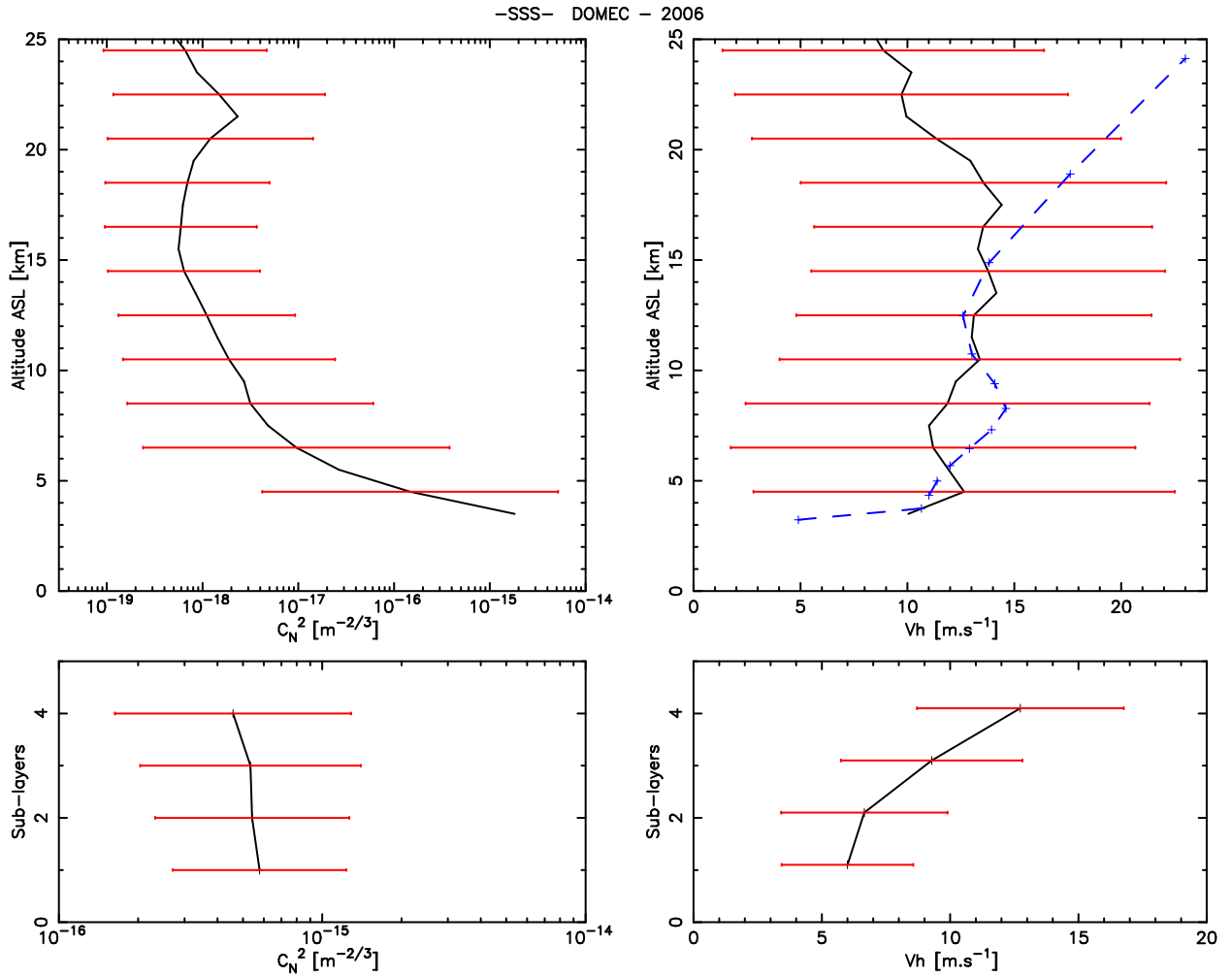


Fig. 8.— Top-left: Median vertical profile of  $C_N^2$  computed by the SSS. Top-right: Average horizontal wind velocity profile (solid line) compared with NOAA archive (dashed line). **Bottom-left: Average  $C_N^2$  within the surface layer (4 sub-layers at the zero altitude).** **Bottom-right: Average horizontal wind speed within the surface layer (4 sub-layers at the zero altitude).** Error bars refer to standard deviation of variable fluctuations.

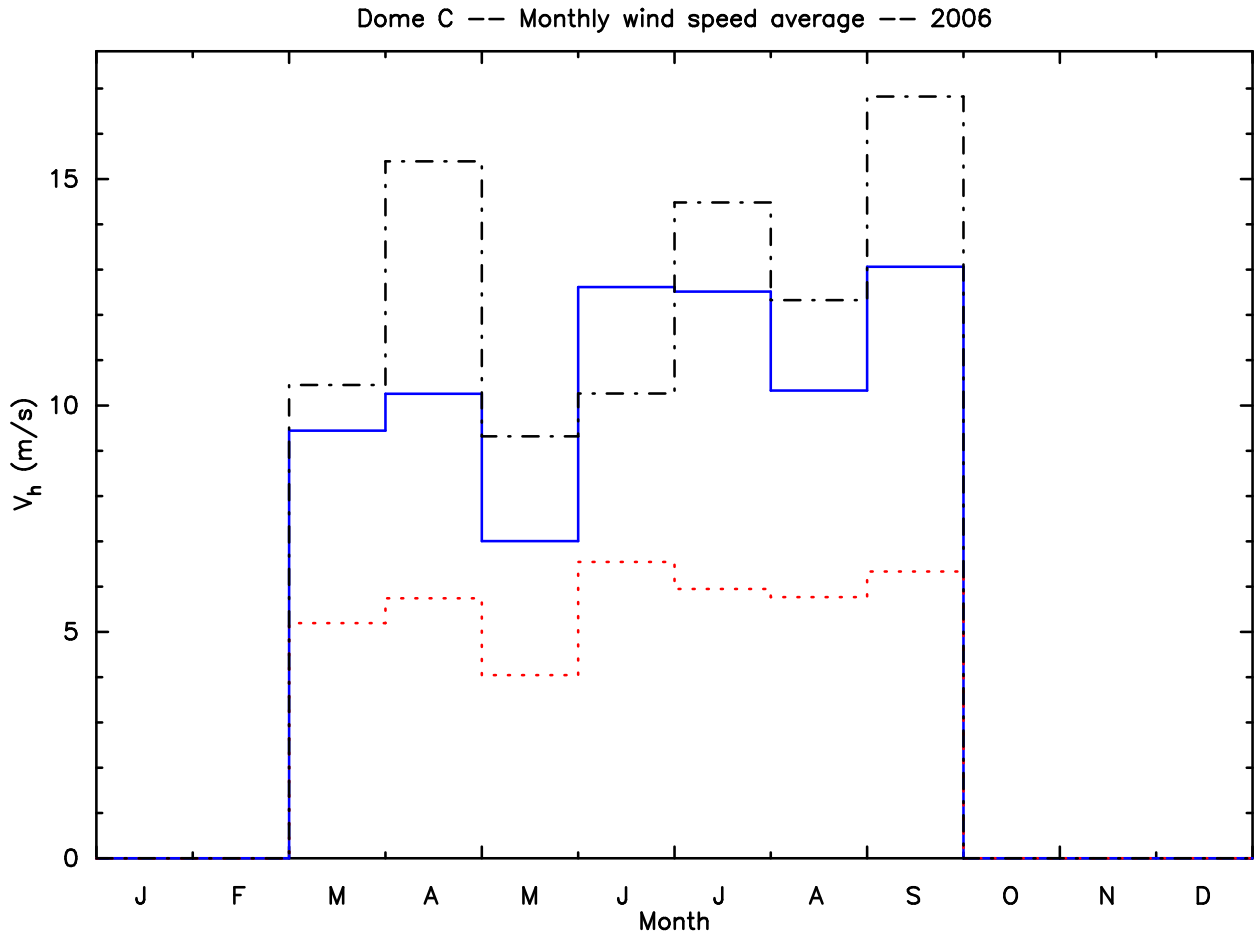


Fig. 9.— Horizontal velocity averaged over the whole atmosphere, monthly computed over 2006 campaign. The dot-dashed line corresponds to the NOAA data, the solid curve corresponds to SSS. The dotted line is the mean velocity of the slowest surface layer measured by the SSS. Zero velocity surface layers have been withdrawn from our statistics considering that they appear in the telescope tube as explained in Vernin et al. (2009). Black columns refers to the number of data taken into account.

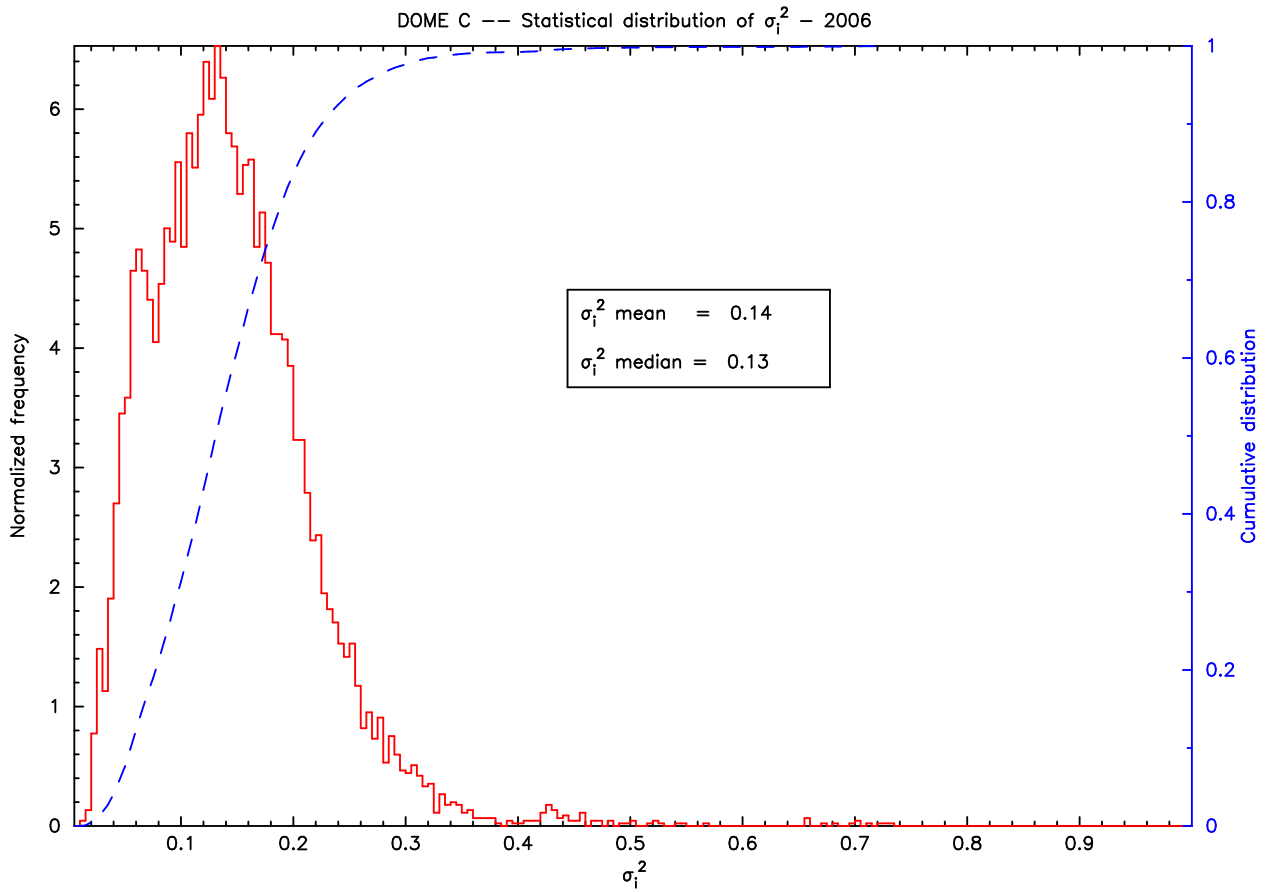


Fig. 10.— Histogram and cumulative distribution of the scintillation index  $\sigma_I^2$  as observed during the whole Dome C campaign in 2006.

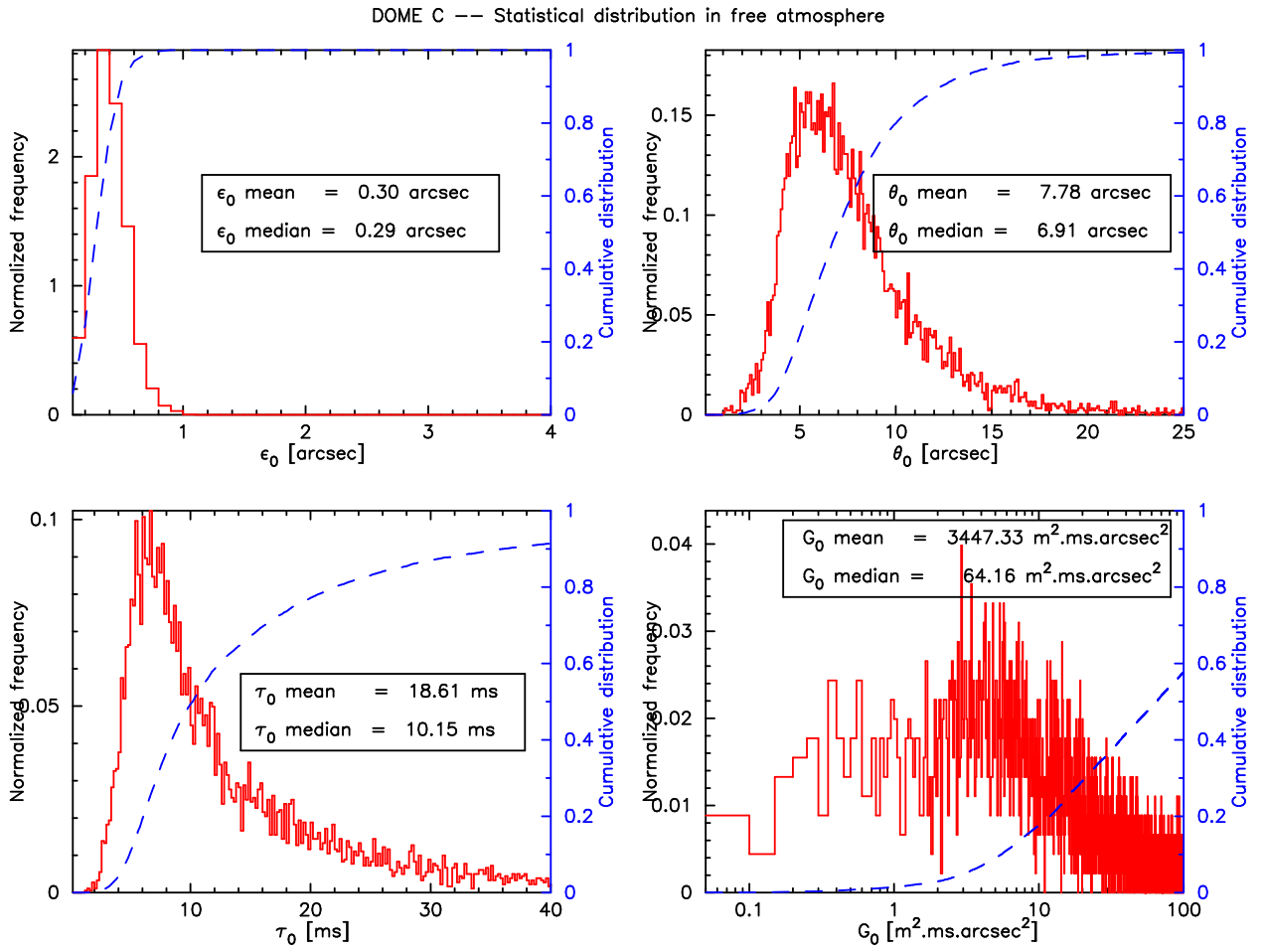


Fig. 11.— Same as Fig. 4, but excluding the surface layer contribution.

<b>Dome C above SL</b>	$\varepsilon_0$	$\theta_0$	$\tau_0$	
<i>this article</i>	0.29	6.9	10.2	median
	0.30	7.8	18.6	mean
<i>Aristidi et al. 2009</i>	0.36	3.9	-	median
<i>Aristidi et al. 2009</i>	0.38	4.3	-	mean
<i>Trinquet et al. 2008</i>	0.4	2.7	6.8	median
<i>Lawrence et al. 2004</i>	0.27	5.7	7.9	mean
<i>Lascaux et al. 2011</i>	0.30	-	-	mean

Table 2: Comparison of  $\varepsilon_0$ ,  $\theta_0$  and  $\tau_0$  computed above the surface layer as measured by various authors at Dome C.

## REFERENCES

- Agabi, A., Aristidi, E., Azouit, M., Fossat, E., Martin, F., Sadibekova, T., Vernin, J., & Ziad, A. 2006, *PASP*, 118, 344
- Aristidi, E., Agabi, A., Fossat, E., Azouit, M., Martin, F., Sadibekova, T., Travouillon, T., Vernin, J., & Ziad, A. 2005, *A&A*, 444, 651
- Aristidi, E., Fossat, E., Agabi, A., Mékarnia, D., Jeanneaux, F., Bondoux, E., Challita, Z., Ziad, A., Vernin, J., & Trinquet, H. 2009, *A&A*, 499, 955
- Geissler, K. & Masciadri, E. 2006, in *Society of Photo-Optical Instrumentation Engineers (SPIE) Conference Series*, Vol. 6267, *Society of Photo-Optical Instrumentation Engineers (SPIE) Conference Series*
- Habib, A., Vernin, J., Benkhaldoun, Z., & Lanteri, H. 2006, *Monthly Not. Roy. Astron. Soc.*, 368, 1456
- Hagelin, S., Masciadri, E., Lascaux, F., & Stoesz, J. 2008, in *Society of Photo-Optical Instrumentation Engineers (SPIE) Conference Series*, Vol. 7012, *Society of Photo-Optical Instrumentation Engineers (SPIE) Conference Series*
- Hoegemann, C. K., Chueca, S., Delgado, J. M., Fuensalida, J. J., Garcia-Lorenzo, B., Mendizabal, E. G., Reyes, M., Verde, M., & Vernin, J. 2004, in *Presented at the Society of Photo-Optical Instrumentation Engineers (SPIE) Conference*, Vol. 5490, *Society of Photo-Optical Instrumentation Engineers (SPIE) Conference Series*, ed. D. Bonaccini Calia, B. L. Ellerbroek, & R. Ragazzoni, 774–784
- Lascaux, F., Masciadri, E., & Hagelin, S. 2011, *MNRAS*, 411, 693
- Lawrence, J. S., Ashley, M. C. B., Bailey, J., Barrado y Navascues, D., Bedding, T. R., Bland-Hawthorn, J., Bond, I., Boulanger, F., Bouwens, R., Bruntt, H., Bunker, A.,

- Burgarella, D., Burton, M. G., Busso, M., Coward, D., Cioni, M.-R., Durand, G., Eiroa, C., Epchtein, N., Gehrels, N., Gillingham, P., Glazebrook, K., Haynes, R., Kiss, L., Lagage, P. O., Le Bertre, T., Mackay, C., Maillard, J. P., McGrath, A., Minier, V., Mora, A., Olsen, K., Persi, P., Pimblet, K., Quimby, R., Saunders, W., Schmidt, B., Stello, D., Storey, J. W. V., Tinney, C., Tremblin, P., Wheeler, J. C., & Yock, P. 2009, *PASA*, 26, 379
- Lawrence, J. S., Ashley, M. C. B., Tokovinin, A., & Travouillon, T. 2004, *Nature*, 431, 278
- Lloyd, J. P. 2004, in *Society of Photo-Optical Instrumentation Engineers (SPIE) Conference Series*, ed. W. A. Traub, Vol. 5491, 190–+
- Marks, R. D., Vernin, J., Azouit, M., Manigault, J. F., & Clevelin, C. 1999, *A&AS*, 134, 161
- Racine, R. 2005, *PASP*, 117, 401
- Roddier, F. 1981, *Prog. Optics*, 19, 281
- Schöck, M., Els, S., Riddle, R., Skidmore, W., Travouillon, T., Blum, R., Bustos, E., Chanan, G., Djorgovski, S. G., Gillett, P., Gregory, B., Nelson, J., Otárola, A., Seguel, J., Vasquez, J., Walker, A., Walker, D., & Wang, L. 2009, *PASP*, 121, 384
- Travouillon, T., Aristidi, E., Fossat, E., Lawrence, J. S., Mekarnia, D., Moore, A. M., Skidmore, A. W., & Storey, J. W. V. 2008, in *Society of Photo-Optical Instrumentation Engineers (SPIE) Conference Series*, Vol. 7012
- Trinquet, H., Agabi, A., Vernin, J., Azouit, M., Aristidi, E., & Fossat, E. 2008, *PASP*, 120, 203
- Vernin, J., Agabi, A., Aristidi, E., Azouit, M., Chadid, M., Fossat, E., Sadibekova, T., Trinquet, H., & Ziad, A. 2007, *Highlights of Astronomy*, 14, 693
- Vernin, J. & Azouit, M. 1983, *Journal d'Optique*, 14, 131

Vernin, J., Chadid, M., Aristidi, E., Agabi, A., Trinquet, H., & van der Swaelmen, M. 2009, *Astron. & Astrophys.*, 500, 1271

Vernin, J., Muñoz-Tuñón, C., Sarazin, M., Vázquez Ramió, H., Varela, A. M., Trinquet, H., Delgado, J. M., Jiménez Fuensalida, J., Reyes, M., Benhida, A., Benkhaldoun, Z., García Lambas, D., Hach, Y., Lazrek, M., Lombardi, G., Navarrete, J., Recabarren, P., Renzi, V., Sabil, M., & Vrech, R. 2011, *PASP*, 123, 1334